Mitigating the Doubly Near–Far Effect in UAV-Enabled WPCN

Hongying Tang, Qingqing Wu, Wen Chen, Jiang Wang, and Baoqing Li

***Abstract*—In this letter, we investigate an unmanned aerial vehicle (UAV) enabled wireless powered communication network (WPCN), in which the UAV first employs the radio frequency (RF) signal to power ground users, and then the users communicate with the UAV by using the harvested energy. The sum rate maximization problem in WPCN suffers doubly near-far effect caused by the double signal propagation loss in both the energy harvesting and communication stage. It is generally believed that this effect can be alleviated by integrating UAV into WPCN, thanks to its flexible deployment. However, due to the lack of analytical solution in state-of-art research, it is still unclear how to quantify the advantage that the mobility of UAV brings to migrating the doubly near-far effect. To address this issue, by showing that the optimal UAV trajectory has a multi-location hovering structure, we first derive the closed-form optimal solution of resource allocation, as a function of the UAV hovering location for downlink wireless power transfer (WPT). We then prove that the UAV in our case only needs to hover at a single location for WPT. More importantly, it is explicitly shown that the doubly near far effect can be alleviated into near-far effect. Simulation results validate our analysis.**

***Index Terms*—Resource allocation, trajectory optimization, wireless powered communication network (WPCN), unmanned aerial vehicle (UAV), sum rate maximization.**

I. Introduction

Internet of Things (IoT), which realizes the connectivity demands of devices, has been greatly benefited from the huge revolution led by the current fifth-generation (5G) developments [1]. To operate IoT in an energy self-sufficient manner, wireless power transfer (WPT) has recently been deemed a promising technology to provide low-power devices with sustainable and controllable energy supply via radio-frequency (RF) transmission from hybrid access points (HAPs) [2]. However, the explosive growth of data requirements in remote areas or emergency network users poses a great challenge for deploying position-fixed HAPs, and thus puts increasing demands on the more flexible robotic platforms. As a sparkling example of robotic platforms, unmanned aerial vehicles (UAVs) will evidently play a critical role in the coming sixth-generation (6 G) integrated ground-water-air-space network, thanks to its advantage of highly controllable mobility and favorable air-ground channels [3]–[6]. It has been envisioned that by integrating UAVs into wireless powered communication network (WPCN), we can realize the Internet of Everything, the advanced version of IoT in 6 G networks [7]. Specifically, much efforts have been devoted in the UAV-enabled WPCN, considering about energy consumption minimization problem [8], [9], transmission completion time minimization [10], energy efficiency maximization [11], etc.

On the other hand, a phenomenon called the doubly near-far effect is reported in WPCNs, that is, the achievable rates of the far-apart users can be quite low since they receive less energy but conversely need to compensate larger distance-based path loss for wireless information transmission (WIT) [12]–[14]. One way to completely overcome the doubly near-far effect, is to care more about the worst-case user and investigate the max-min rate problem as in [12], [13]. Using the Lagrange dual method, it was shown in [12] that when the UAV speed is sufficiently large, the optimal UAV trajectory follows a multi-location-hovering structure, where the UAV hovers at a system-dependent number of locations with optimized hovering durations. However, the dual variables in [12] are updated by the subgradient-based method, which leads to prohibitively complexity especially when the network size is large. Later in [13], the multi-location hovering structure of UAV was extended to the UAV-enabled WPCN interference channel, for a toy example of two users.

As another important metric of rate maximization problem in WPCNs, sum rate maximization problem of joint UAV position and resource allocation was studied in [14]–[16]. The authors of [14] proposed a weighted-harvest-then-transmit protocol, where an HAP-equipped UAV performs the assistant of the fixed HAP, by providing weighted wireless power transfer (WPT) and helping far-apart users for data collection. For a UAV-enabled full-duplex WPCN, the authors in [15] maximized the network throughput through resource allocation optimization, where the energy transfer and information communication tasks at UAV are executed simultaneously. However, the WPCN model in [15] only considered the over-simplified one-dimensional sensor distribution. Although the above aforementioned work can mitigate the doubly near-far effect to a certain extent, the technical role that the UAV plays in mitigating this effect is unclear due to lack of a closed-form solution and the coexistence of the full-duplex manner or the fixed HAP. Unfortunately, as we will show later, without any external assistance, deploying a static half-duplex UAV as in [16] provides no benefit to alleviate the doubly near-far effect. As such, one natural question to ask is how to efficiently mitigate this effect by leveraging the mobility of a single half-duplex UAV in the sum rate maximization problem.

To answer this question, in this letter, we study the doubly near-far effect in sum rate maximization problem by dynamically adjusting the UAV's trajectory to get close to users in WPCN. This problem can be solved via the Lagrange duality method since it satisfies the time-sharing condition. By convincing the multi-location-hovering structure of the optimal UAV trajectory, we innovatively represent the dual variables and resource allocation as a function of the UAV hovering location for WPT. We further unveil that there exists an optimal UAV hovering scheme, whose number of locations is just one more than that of ground users. By presenting the closed form solution of joint trajectory and resource allocation, it is analytically shown that the proposed dynamic scheme not only achieves significant sum rate improvement over static

Manuscript received January 26, 2021; revised May 7, 2021 and June 18, 2021; accepted July 8, 2021. Date of publication July 14, 2021; date of current version August 13, 2021. This work was supported in part by NSFC under Grant 61901457, in part by Macau Science and Technology Development Fund, under Grants 0119/2020/A3 and 0108/2020/A, in part by Guangdong NSF under Grant 2021A1515011900, in part by National Key Project under Grants 2018YFB1801102 and 2020YFB1807700, in part by NSFC under Grant 62071296, in part by STCSM under Grant 20JC1416502, and in part by the Innovation Foundation of Chinese Academy of Sciences under Grant CXJJ-20S037. The review of this article was coordinated by Prof. Witold A Krzymien. *(Corresponding author: Qingqing Wu.)*

Hongying Tang, Jiang Wang, and Baoqing Li are with the Science and Technology on Microsystem Laboratory, Shanghai Institute of Microsystem and Information Technology, Chinese Academy of Sciences, Shanghai 200050, China (e-mail: tanghy@mail.sim.ac.cn; jiang.wang@mail.sim.ac.cn; sinoiot@mail.sim.ac.cn).

Qingqing Wu is with the State Key Laboratory of Internet of Things for Smart City, University of Macau, Macau 999078, China (e-mail: qingqingwu@um.edu.mo).

Wen Chen is with the Department of Electronic Engineering, Shanghai Jiaotong University, Shanghai 200240, China (e-mail: wenchen@sjtu.edu.cn).

Digital Object Identifier 10.1109/TVT.2021.3096540

scheme in [16], but also alleviates the doubly near-far effect into the near-far effect.

II. System Model and Problem Formulation

Consider a UAV-enabled WPCN, where a UAV is dispatched to periodically charge a set $\mathcal{K} \triangleq \{1, \ldots, K\}$ of ground users via WPT in the downlink, and each user $k \in \mathcal{K}$ uses its harvested energy to send its information to the UAV in the uplink.

The UAV flies horizontally at a fixed altitude $H > 0$ in meter (m), over a finite flight period $\mathcal{T} \in [0, T]$ with T in seconds (s). At any given time instant $t \in \mathcal{T}$, let $\mathbf{q}(t)$ denote the location of the UAV projected on the horizontal plane. Since the air-to-ground channel has LoS-dominated links, especially for rural areas, we adopt free-space path loss model as in [10], [12], [16].[1] Furthermore, we assume that the Doppler effect has been perfectly compensated at the ground users. Suppose that each user $k \in \mathcal{K}$ is at a fixed location $\mathbf{w}_k$ on the ground in a two-dimensional (2D) Cartesian coordinate system, which is a priori known by the UAV. Then the channel power gain from the UAV to user k in time t can be expressed as $h_k(t) = \frac{\beta_0}{H^2 + \|\mathbf{q}(t) - \mathbf{w}_k\|^2}$, where $\sqrt{H^2 + \|\mathbf{q}(t) - \mathbf{w}_k\|^2}$ denotes the distance from the UAV to user k in time t, and β_0 denotes the channel power gain at the reference distance $d_0 = 1$ m.

Assume that the both the WPT and WIT stages operate in a time division multiple access (TDMA) manner. At each time instant $t \in \mathcal{T}$, we use the binary indicators $z_0(t) = 1$ and $z_k(t) = 0$, $\forall k \in \mathcal{K}$, to indicate the downlink WPT mode; while use $z_k(t) = 1$, $k \in \mathcal{K}$ and $z_j(t) = 0, \forall j \in \{0\} \cup \mathcal{K}, j \neq k$, to represent the uplink WIT mode. It then follows that

$$\sum_{k=0}^{K} z_k(t) = 1, z_k(t) \in \{0, 1\}, \forall k \in \{0\} \cup \mathcal{K}, \forall t \in \mathcal{T}. \tag{1}$$

Due to the broadcast nature of wireless transmission, all ground users can simultaneously receive wireless power during the WPT mode. Hence, the energy received by ground user k is given by $E_k^R = \int_0^T \frac{\eta \beta_0 P z_0(t)}{\|\mathbf{q}(t) - \mathbf{w}_k\|^2 + H^2} dt$, where $0 \leq \eta \leq 1$ denotes the energy conversion efficiency at the energy harvester of each user and P denotes the constant WPT power of UAV. Denote the transmit power of user k at time $t \in \mathcal{T}$ by $p_k(t) \geq 0$. Then the energy consumption of node k is given by $E_k^O = \int_0^T z_k(t) p_k(t) dt$. We assume that the users have sufficiently large battery capacities. In this case, as long as the energy neutrality constraints $E_k^R \geq E_k^O$, or i.e.,

$$\int_0^T z_k(t) p_k(t) dt \leq \int_0^T \frac{\eta \beta_0 P z_0(t)}{\|\mathbf{q}(t) - \mathbf{w}_k\|^2 + H^2} dt, \forall k \in \mathcal{K}, \tag{2}$$

hold over each period, each user can operate perpetually.

Accordingly, the instantaneous achievable rate of user k in time $t \in \mathcal{T}$, denoted by $r(t)$ in bps/Hz, can be expressed as $r_k(t) = z_k(t) \log_2(1 + \frac{\gamma p_k(t)}{\|\mathbf{q}(t) - \mathbf{w}_k\|^2 + H^2})$, where $\gamma \triangleq \frac{\beta_0}{\sigma^2}$ and σ^2 is the noise power at the UAV. As a result, the sum rate of all users over the flight period, is given by $R_{\text{sum}} = \frac{1}{T} \sum_{k=1}^{K} \int_0^T z_k(t) \log_2(1 + \frac{\gamma p_k(t)}{\|\mathbf{q}(t) - \mathbf{w}_k\|^2 + H^2}) dt$.

[1] Although more complicated channel models have been investigated in the literature, the real-time performance guarantee is sacrificed in favour of average performance. Moreover, it is infeasible to obtain the time-varying small-scale channel fading before UAV's flight. Therefore, we adopt the LoS channel here to gain the most essential design insights. The more general fading channel considering both large-scale and small-scale fading is left for our future work.

To maximize the sum rate among K users via jointly optimizing the resource allocation and the UAV trajectory, the mathematical problem is formulated as

$$(\mathcal{Q}): \max_{\{\mathbf{q}(t), p_k(t), z_k(t)\}_{t=0}^T} R_{\text{sum}}$$
$$\text{s.t.} \quad (1), (2), \tag{3a}$$
$$p_k(t) \geq 0, \forall k \in \mathcal{K}, t \in \mathcal{T}. \tag{3b}$$
$$\|\dot{\mathbf{q}}(t)\| \leq V_{\max}. \tag{3c}$$
$$\mathbf{q}(0) = \mathbf{q}(T). \tag{3d}$$

where (3c) denotes the UAV's maximum speed constraint, and (3d) implies that the UAV serves ground users periodically.

In this work, since we discuss the best effort to mitigate the doubly near-far effect in sum rate maximization problem, we assume that the ideal case when $V_{\max}$ is sufficiently large, and drop constraints (3c) as in [10], [12], [13]. Then problem $(\mathcal{Q})$ becomes

$$(\mathcal{P}): \max_{\{\mathbf{q}(t), p_k(t), z_k(t)\}_{t=0}^T} R_{\text{sum}}$$
$$\text{s.t.} \quad (1), (2), (3b).$$

where we have omitted constraint (3d) since it can be easily satisfied for sufficiently large $V_{\max}$. Note that the optimal value of problem $(\mathcal{P})$ is the upper bound of problem $(\mathcal{Q})$ for any given $V_{\max}$, which is asymptotically achievable by a practical scheme as shown in the simulations.

III. Efficient Solution of Problem $(\mathcal{P})$

It can be observed that problem $(\mathcal{P})$ is a non-convex problem with infinite-dimension variables $\{\mathbf{q}(t), p_k(t), z_k(t)\}_{t=0}^T$, which makes it difficult to find a globally optimal solution. However, it satisfies the time-sharing condition in [17], suggesting a zero duality gap between problem $(\mathcal{P})$ and its Lagrange dual problem. Therefore, the Lagrange duality based method in [12] (referred as "LD Method" in the following text) applies here. In the following, we first briefly outline the LD Method, then present a semi-closed form solution by exploring the specific structure of problem $(\mathcal{P})$.

A. LD Method

Denote $\tilde{P} \triangleq \eta \beta_0 P$, and $\boldsymbol{\mu} \triangleq [\mu_1, \ldots, \mu_K]^T \succeq 0$ as the Lagrange multiplier associated with constraints in (2). As in [12], the Lagrange dual function of problem $(\mathcal{P})$ is given by

$$\max_{\{\mathbf{q}(t), p_k(t), z_k(t)\}_{t=0}^T} \mathcal{L}(\{\mathbf{q}(t), p_k(t), z_k(t)\}, \boldsymbol{\mu}),$$
$$\text{s.t.} \quad (1), (3b). \tag{4}$$

where

$$\begin{aligned}
&\mathcal{L}(\{\mathbf{q}(t), p_k(t), z_k(t)\}_{t=0}^T, \boldsymbol{\mu}) \\
&= \sum_{k=1}^{K} \frac{1}{T} \int_0^T \log_2 \left(1 + \frac{\gamma p_k(t)}{\|\mathbf{q}(t) - \mathbf{w}_k\|^2 + H^2}\right) z_k(t) dt \\
&- \sum_{k=1}^{K} \mu_k \left(\int_0^T z_k(t) p_k(t) dt - \int_0^T \frac{\tilde{P} z_0(t)}{\|\mathbf{q}(t) - \mathbf{w}_k\|^2 + H^2} dt \right) \\
&= \int_0^T \sum_{k=1}^{K} z_k(t) \phi(\mathbf{q}(t), p_k(t), \mu_k) + z_0(t) \psi(\mathbf{q}(t), \boldsymbol{\mu}) dt,
\end{aligned}$$

where $\phi(\mathbf{q}(t), p_k(t), \mu_k) \triangleq \frac{1}{T}\log_2(1+\frac{\gamma p_k(t)}{\|\mathbf{q}(t)-\mathbf{w}_k\|^2+H^2}) - \mu_k p_k(t)$, and $\psi(\mathbf{q}(t), \boldsymbol{\mu}) \triangleq \sum_{k=1}^{K} \frac{\tilde{P}\mu_k}{\|\mathbf{q}(t)-\mathbf{w}_k\|^2+H^2}$. Accordingly, problem (4) can be decomposed into an infinite number of subproblems over continuous time, which can be thus re-expressed as

$$g(\boldsymbol{\mu}) \triangleq \max_{\{\mathbf{q}, p_k, z_k\}} \sum_{k=1}^{K} z_k \phi(\mathbf{q}, p_k, \mu_k) + z_0 \psi(\mathbf{q}, \boldsymbol{\mu}) \quad \text{s.t.} \quad (1), (3b). \tag{5}$$

According to constraint (1), there are $K+1$ feasible $\{z_k\}$ to consider in total. First, consider the case when $z_k = 1$ for a certain $k \in \mathcal{K}$ and $z_j = 0$, $\forall j \in \{0\} \cup \mathcal{K}, j \neq k$. Then problem (5) can be reformulated as

$$\max_{\{\mathbf{q}, p_k\}} \phi(\mathbf{q}, p_k, \mu_k) \quad \text{s.t. } (3b). \tag{6}$$

With given μ_k, the optimal solution of problem (6) is given by $\mathbf{q}^\star = \mathbf{w}_k$, $p_k^\star = \frac{H^2}{\gamma}(\frac{\kappa}{\mu_k} - 1)^+$, with the corresponding optimal value given by

$$\vartheta(\mu_k) \triangleq \phi(\mathbf{q}^\star, p_k^\star, \mu_k) = \begin{cases} \frac{H^2}{\gamma}\left(\kappa \ln(\frac{\kappa}{\mu_k}) - (\kappa - \mu_k)\right), 0 \le \mu_k < \kappa, \\ 0, \quad \mu_k \ge \kappa, \end{cases}$$

where $\kappa \triangleq \frac{\gamma}{TH^2 \ln 2}$. Next, consider the case when $z_0 = 1$ and $z_k = 0$, $\forall k \in \mathcal{K}$. In the case, problem (5) can be reformulated as $f(\boldsymbol{\mu}) \triangleq \max_{\mathbf{q}} \psi(\mathbf{q}, \boldsymbol{\mu})$, whose optimal solution can be denoted as $\mathbf{q} = \bar{\mathbf{q}}_\omega^\mu$, $\omega \in \{1, \ldots, \Omega^\mu\}$. Then the dual problem of problem $(\mathcal{P})$ is given by

$$(\mathcal{D}1): \min_{\boldsymbol{\mu} \in \mathcal{X}} \sum_{k=1}^{K} z_k^\star \vartheta(\mu_k) + z_0^\star f(\boldsymbol{\mu}) \tag{7}$$

where $z_k^\star$, $k \in \{0\} \cup \mathcal{K}$ is the optimal solution of problem (5) and $\mathcal{X} \triangleq \{\boldsymbol{\mu} | \mu_k \ge 0, \forall k \in \mathcal{K}\}$. Then the optimal $\boldsymbol{\mu}^\star$ is determined by using subgradient-based methods. The optimal UAV follows the multi-location-hovering structure: it successively hovers above $\{\mathbf{w}_1, \ldots, \mathbf{w}_K, \bar{\mathbf{q}}_1, \ldots, \bar{\mathbf{q}}_\Omega^{\mu^\star}\}$, where in the flight duration is determined by a time-sharing operation. For the overall algorithm, please refer to [12].

B. Closed Form Solution

In this subsection, we first derive that the optimal solution of $\boldsymbol{\mu}$ as a function of the UAV hovering location for WPT. Then we show that there exists an optimal UAV hovering scheme with $K+1$ hovering locations. Define C as the maximum value of the following problem

$$\max_{\mathbf{q}} \sum_{k=1}^{K} \frac{\tilde{P}}{\|\mathbf{q}-\mathbf{w}_k\|^2 + H^2}. \tag{8}$$

Proposition 1: The optimal solution of problem $(\mathcal{D}1)$ is given by $\boldsymbol{\mu}^\star = [\mu^\star, \ldots, \mu^\star]^T$, $\vartheta(\mu^\star) = f(\boldsymbol{\mu}^\star)$, where $\mu^\star = \frac{\kappa \mathcal{W}(\frac{\tilde{C}-1}{e})}{\tilde{C}-1}$ and $\tilde{C} \triangleq \frac{\gamma}{H^2}C$.

Proof: See Appendix A. ∎

Proposition 1 implies that when the UAV works at the WIT mode, the optimal transmit power of each user is given by

$$p^\star = \frac{H^2}{\gamma}\left(\frac{\tilde{C}-1}{\mathcal{W}(\frac{\tilde{C}-1}{e})} - 1\right), \tag{9}$$

with the corresponding individual rate given by $r^\star = \log_2(1+\frac{\gamma p^\star}{H^2}) = \log_2(\frac{\kappa}{\mu^\star})$. In light of the derivation of problem (5), we can know that the optimal UAV trajectory for WIT stage is $\mathbf{q}^\star = \mathbf{w}_k$. This indicates that the user-to-UAV communication only happens when the UAV hovers exactly above each user, with fixed power $p^\star$. Therefore, the transmission outage will never happen. One can infer that the rate difference between each user comes from the different hovering duration of the UAV.

Remark 1: In the above, we have proved that the optimal UAV trajectory is independent from the resource allocation through three steps: First, the optimal UAV trajectory can be determined by time-sharing the optimal hovering locations for WPT and WIT; Second, according to the derivation of problem (5), the UAV hovering locations for WIT are the K user positions; Finally, Proposition 1 decomposes the association between optimal hovering locations for WPT and resource allocation.

Denote the optimal solution in problem (8) as $\mathbf{q} = \mathbf{x}_\omega$, $\omega \in \{1, \ldots, \Omega\}$. Since Ω can be larger than 1, to construct the optimal primal solution, we need to time-share among $\{\mathbf{w}_1, \ldots, \mathbf{w}_K, \mathbf{x}_1, \ldots, \mathbf{x}_\Omega\}$. Specifically, let π_ω and τ_k denote the normalized time-sharing factor associated with the hovering location at $\mathbf{x}_\omega$, $\omega = 1, \ldots, \Omega$ and $\mathbf{w}_k$, $k \in \mathcal{K}$, respectively. Let $\mathbb{R}^N$ denote the N-dimensional real field. Defining $\boldsymbol{\tau} \triangleq [\tau_1, \ldots, \tau_K]^T \in \mathbb{R}^K$, $\boldsymbol{\pi} \triangleq [\pi_1, \ldots, \pi_\Omega]^T \in \mathbb{R}^\Omega$ and $\theta_{k\omega} = \frac{\tilde{P}}{\|\mathbf{x}_w - \mathbf{w}_k\|^2 + H^2}$, we have

$$\max_{\boldsymbol{\tau}, \boldsymbol{\pi}} \sum_{k=1}^{K} r^\star \tau_k$$

$$\text{s.t. } p^\star \tau_k \le \sum_{\omega=1}^{\Omega} \theta_{k\omega} \pi_\omega, \forall k, \tag{10a}$$

$$\sum_{k=1}^{K} \tau_k + \sum_{\omega=1}^{\Omega} \pi_\omega = 1, \tag{10b}$$

$$\tau_k \ge 0, \pi_\omega \ge 0, \forall k, \omega. \tag{10c}$$

Proposition 2: The optimal value in problem (10) is a function of $\tilde{C}$, which is given by $R_{\text{sum}}^\star(\tilde{C}) = \frac{\tilde{C}\mathcal{W}(\frac{\tilde{C}-1}{e})}{\ln 2(\tilde{C}-1)}$, and be achieved by arbitrarily choosing $\hat{\omega}$, $1 \le \hat{\omega} \le \Omega$, and set $\tau_k^\star = \frac{\theta_{k\hat{\omega}}}{C+p^\star}$, $\pi_{\hat{\omega}}^\star = \frac{p^\star}{C+p^\star}$, and $\pi_\omega^\star = 0, \forall \omega \neq \hat{\omega}$.

Proof: See Appendix B. ∎

Based on Proposition 2, the remaining challenge is to solve problem (8), which can be determined by the 2D exhaustive search or the global optimal method in [16]. For the overall trajectory and resource allocation design of problem $(\mathcal{P})$, divide the whole flight time into $K+1$ slots, where in the first slot $\mathcal{T}_1 = (0, \pi_{\hat{\omega}}]$, the UAV hovers above $\mathbf{x}_{\hat{\omega}}$ for WPT; while in the next K slots, denoted by $\mathcal{T}_{k+1} = (\pi_{\hat{\omega}} + \sum_{j=1}^{k-1}\tau_k, \pi_{\hat{\omega}} + \sum_{j=1}^{k}\tau_k]$, $k \in \mathcal{K}$, the UAV successively hovers above $\mathbf{w}_k$ for WIT.

Remark 2: For a K-user network with different locations, we can show that problem $(\mathcal{P})$ achieves higher R_{sum} that in [16]. Denote $\bar{\mathbf{q}}$ and A as the optimal solution and value of $\max_{\mathbf{q}} \sum_{k=1}^{K} \frac{\tilde{P}}{(\|\mathbf{q}-\mathbf{w}_k\|^2+H^2)^2}$, respectively. The optimal R_{sum} in [16] is given by $R_{\text{sum}}^\star(\tilde{A}) = \frac{\tilde{A}\mathcal{W}(\frac{\tilde{A}-1}{e})}{\ln 2(\tilde{A}-1)}$, where $\tilde{A} = \gamma A$. Then we have $\tilde{A} = \max_{\mathbf{q}} \sum_{k=1}^{K} \frac{\gamma\tilde{P}}{(\|\mathbf{q}-\mathbf{w}_k\|^2+H^2)^2} = \sum_{k=1}^{K} \frac{\gamma\tilde{P}}{(\|\bar{\mathbf{q}}-\mathbf{w}_k\|^2+H^2)^2} \le \sum_{k=1}^{K} \frac{\gamma\tilde{P}}{(\|\bar{\mathbf{q}}-\mathbf{w}_k\|^2+H^2)H^2} \le \max_{\mathbf{q}} \sum_{k=1}^{K} \frac{\gamma\tilde{P}}{(\|\mathbf{q}-\mathbf{w}_k\|^2+H^2)H^2} = \frac{\gamma C}{H^2} = \tilde{C}$. since $R_{\text{sum}}^\star(x)$ is increasing with respect to x, we have $R_{\text{sum}}^\star(\tilde{A}) \le R_{\text{sum}}^\star(\tilde{C})$. The equality can only be achieved when $\mathbf{w}_1 = \cdots = \mathbf{w}_K$.

Remark 3: Notice that the optimal resource allocation is determined by (9) and Proposition 2. The only computational intensive operation in our method comes from the derivation of WPT hovering location in problem (8). For a 200×200 meters square area, the computational complexity is $\mathcal{O}(\frac{200}{\varepsilon} \cdot \frac{200}{\varepsilon})$, where ε denotes the precision over x-axis and y-axis. However, this operation only has to compute once. By comparison, in "LD Method," problem $(\mathcal{D}1)$ has to be computed for each update of $\boldsymbol{\mu}$. As such, its complexity is given by $\mathcal{O}(K^2(\frac{200}{\varepsilon} \cdot \frac{200}{\varepsilon})) + \mathcal{O}(K + \Omega^\star)$, where $O(K + \Omega^\star)$ is the complexity for time-sharing operation. Obviously, our proposed method greatly simplifies the computation complexity.

C. Doubly Near-Far Effect

In this subsection, we will show that by maneuvering the mobility of UAV, the doubly near-far effect can be alleviated into near-far effect.

Doubly near-far effect arises from unequal distances between each user and the fixed HAP, which significantly deteriorates fairness among them. For the static UAV case in [16], the optimal rate of user k is proportional to $\frac{1}{(\|\mathbf{x}^\sharp - \mathbf{w}_k\|^2 + H^2)^2}$, where $\mathbf{x}^\sharp$ is the optimal UAV hovering location. Accordingly, the user rate suffers twofold degradation due to signal propagation loss coming from the energy harvesting as well as the information transmission. This implies that once the position of HAP is fixed (no matter whether it can be flexibly deployed or not), the doubly near-far effect cannot be alleviated only by adjusting the resource allocation.

In contrast, for our dynamic UAV case, by maneuvering equivalent distance over time between the UAV and each user in the uplink, the communication rate only depends on the harvested energy. As illustrated in Proposition 2, the optimal rate of user k is proportional to $\frac{1}{\|\mathbf{x}_w - \mathbf{w}_k\|^2 + H^2}$, which typically shows near-far effect rather than the doubly near-far effect. Therefore, the twofold degradation reduces to one fold degradation due to energy harvesting loss.

IV. Simulation Results

In this section, we present our simulation results to evaluate the performance of our proposed scheme. Consider a system with K users randomly distributed in a 200×200 square meter range. The system parameters are: $P = 20$dBm, $P_{\max} = -10$ dBm, $\sigma^2 = -169$dBm, $\beta_0 = -50$dB, $V_{\max} = 40$m/s and $\eta = 0.5$. The UAV flight hight is set as 50 m unless otherwise stated.

To deal with problem $(\mathcal{Q})$, we propose a successive hover-and-fly trajectory solution (SHAF), where the UAV sequentially flies towards $\{\mathbf{x}_{\hat{\omega}}, \mathbf{w}_1, \ldots, \mathbf{w}_K\}$ with the minimum distance at constant speed $V_{\max}$ for WPT and WIT, and returns to the starting point when the flight mission ends. The flying distance minimization and resource allocation problem can be determined following similar steps in [12]. Note that SHAF provides a practical way to implement problem $(\mathcal{P})$ by taking into account the UAV speed constraint. We compare the following schemes: 1) DanH: the proposed dynamic hovering scheme in Proposition 2 (without velocity constraint); 2) SHAF; 3) MaxMin: minimum-rate maximization scheme in [12] (without velocity constraint). 4) StaH: static hovering scheme in [16].

First, we provide the computation time of problem $(\mathcal{P})$ versus the number of ground users in Table I. We can see that our proposed scheme requires much lower computational time than "LD Method," which convinces the complexity analysis in Section III-C. This is expected since our proposed scheme gives a semi-closed form solution, while "LD Method" is iterative, which converges slowly when K becomes large.

TABLE I
THE AVERAGE COMPUTATION TIME COMPARISON (IN SECONDS)

K	3	4	5	6	7	8
Proposed Scheme	0.05	0.06	0.07	0.07	0.08	0.09
LD Method	8.44	20.91	37.15	60.26	91.21	131.50

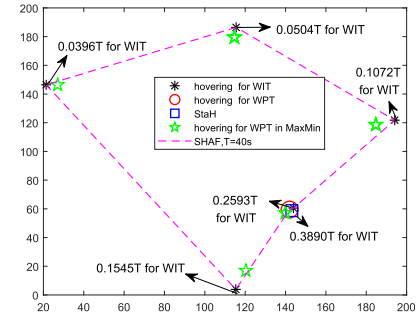

(a)

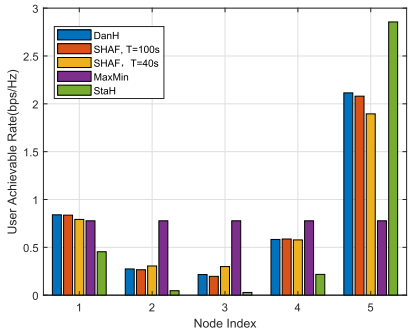

(b)

Fig. 1. (a) Optimized UAV trajectory when $K = 5$, (b) Individual rate of each user when $K = 5$.

Fig. 1(a) shows the UAV trajectory with $K = 5$ users, whose locations are given by $[115.34, 3.88]^T$m, $[115.51, 186.43]^T$m, $[21.37, 146.43]^T$m, $[194.10, 121.77]^T$m and $[143.93, 60.44]^T$m, respectively. For brevity, we only plot the optimized time allocation for WIT and WPT of DanH. It can be found that the UAV allocates the most time for WIT with the user that is closest to the hovering location for WPT. We also observe that there is only one optimal hovering location for WPT in DanH, which is almost overlapped with that in StaH. That is, $\mathbf{x}_w \approx \mathbf{x}^\sharp$. By comparison, there are 5 hovering locations in MaxMin for WPT. Fig. 1(b) shows the individual rate of each user. We can see that MaxMin strikes a balance between the rate of each user, due to the fact that their objective is to resolve the user fairness issue. Denote ρ as the ratio of the maximum user rate to the minimum user rate. Then $\rho_{\text{DanH}} = \frac{\max_k \|\mathbf{x}_w - \mathbf{w}_k\|^2 + H^2}{\min_k \|\mathbf{x}_w - \mathbf{w}_k\|^2 + H^2} = 9.8244$. Therefore, $\rho_{\text{StaH}} = (\frac{\max_k \|\mathbf{x}^\sharp - \mathbf{w}_k\|^2 + H^2}{\min_k \|\mathbf{x}^\sharp - \mathbf{w}_k\|^2 + H^2})^2 = 99.9765$ approximately doubles ρ_{DanH}. As such, DanH shows more balanced user rates than that in StaH, which justifies our motivation by alleviating the severe user unfairness issue.

Fig 2 shows the sum rate comparison versus K and H, respectively. It can be observed that the performance of our proposed scheme is almost achieved by that of SHAF when $T = 100\,s$. Furthermore, both schemes significantly outperform Maxmin and StaH, which validates the advantage of our scheme. We can also observe that sum rate increases with the increase of K. This result can be expected since more K needs more hovering locations, i.e., more flexibility, which

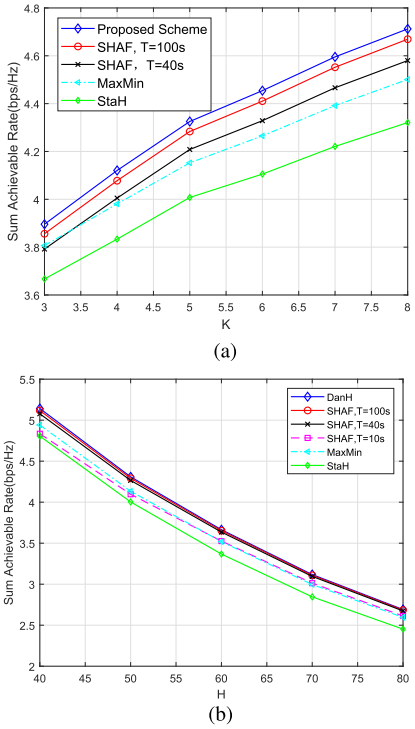

Fig. 2. (a) R_{sum} versus K, (b) R_{sum} versus H.

can be provided by our proposed scheme. As expected, the increase of H gives a negative impact on the sum rate. The reason is that, larger H not only leads to less harvested energy, but also results in larger distance-based path loss for communication.

V. Conclusion

In this paper, we have investigated the sum rate maximization problem in the UAV-enabled WPCN by joint design of the UAV trajectory and resource allocation. The optimal UAV trajectory exhibits a multi-location hovering structure as in [12], but with fewer hovering locations. It is also shown that the proposed scheme not only achieves significant sum rate improvement over static scheme in [16], but also alleviates the doubly near-far effect into the near-far effect, both analytically and numerically.

This work does not consider the energy constraint of UAV. However, as mentioned in [8], [9], the UAV trajectory needs more delicate design under limited onboard energy, to guarantee the flight task for energy transfer and information communication. Furthermore, the average energy constraint in (2) does not always ensure perpetual operations of ground users, which may weaken the usefulness of WPT. How to mitigate the doubly near-far effect by taking into account the above practical considerations is challenging and worth pursuing for future investigation.

Appendix A
Proof of Proposition 1

In problem $(D1)$, when $f(\boldsymbol{\mu}) \geq \vartheta(\mu_k)$, $\forall k \in \mathcal{K}$, we can easily know that $z_0^\star = 1$ by the definition of $g(\boldsymbol{\mu})$. Otherwise, $z_k^\star = 1$, for $k = \arg\max\{\vartheta(\mu_1), \ldots, \vartheta(\mu_K)\}$. This leads to the equivalent expression of problem $(\mathcal{D}1)$ as

$$(\mathcal{D}2): \min_{\boldsymbol{\mu}\in\mathcal{X}} \max\left\{\vartheta(\mu_1), \ldots, \vartheta(\mu_K), f(\boldsymbol{\mu})\right\}.$$

To prove Proposition 1, we need the following Lemma.

Lemma 1: Define $\boldsymbol{\mu}' \triangleq [\mu_1', \ldots, \mu_K']^T$ and $\boldsymbol{\mu}'' \triangleq [\mu_1'', \ldots, \mu_K'']^T$. If $\mu_k' \leq \mu_k''$ for $\forall k \in \mathcal{K}$ and $\mu_k' < \mu_k''$ for some $k \in \mathcal{K}$, then $f(\boldsymbol{\mu}') < f(\boldsymbol{\mu}'')$.

Proof: Denote $\mathbf{q}' = \arg\max_{\mathbf{q}} \psi(\mathbf{q}, \boldsymbol{\mu}')$. Then we have $f(\boldsymbol{\mu}') = \max_{\mathbf{q}} \sum_{k=1}^K \frac{\mu_k'}{\|\mathbf{q}-\mathbf{w}_k\|^2+H^2} = \sum_{k=1}^K \frac{\mu_k'}{\|\mathbf{q}'-\mathbf{w}_k\|^2+H^2} \leq \sum_{k=1}^K \frac{\mu_k''}{\|\mathbf{q}'-\mathbf{w}_k\|^2+H^2} \leq \max_{\mathbf{q}} \sum_{k=1}^K \frac{\mu_k''}{\|\mathbf{q}-\mathbf{w}_k\|^2+H^2} = f(\boldsymbol{\mu}'')$, which completes the proof. ■

Based on Lemma 1, we next show by contradiction that the optimal solution in problem $(\mathcal{D}2)$ must have $\mu_1^\star = \cdots = \mu_K^\star$ and $\vartheta(\mu_k^\star) = f(\boldsymbol{\mu}^\star)$, for $\forall k \in \mathcal{K}$. Define $\boldsymbol{\mu}^\star \triangleq [\mu_1^\star, \ldots, \mu_K^\star]^T$ as the optimal solution of problem $(\mathcal{D}2)$, and $\mathcal{K}' \triangleq \{k | k = \arg\max \vartheta(\mu_k^\star), k \in \mathcal{K}\}$.[2] Suppose that $\mathcal{K}' \neq \mathcal{K}$, then there exits some $j \in \mathcal{K} \setminus \mathcal{K}'$ such that $\vartheta(\mu_{k'}^\star) > \vartheta(\mu_j^\star)$ (or [3] $\mu_{k'}^\star < \mu_j^\star$). Next we consider the following two cases.

First, consider $\vartheta(\mu_{k'}^\star) < f(\boldsymbol{\mu}^\star)$. That is, $f(\boldsymbol{\mu}^\star) = \max\{\vartheta(\mu_1^\star), \ldots, \vartheta(\mu_K^\star), f(\boldsymbol{\mu}^\star)\}$. We can always find a new solution $\boldsymbol{\mu}^\circ = [\mu_1^\circ, \ldots, \mu_K^\circ]^T$, i.e., $\mu_j^\circ = \mu_j^\star - \varepsilon_j, \forall j \in \mathcal{K} \setminus \mathcal{K}', \mu_{k'}^\circ = \mu_{k'}^\star, \forall k' \in \mathcal{K}'$, where ε_j is sufficiently small such that $\mu_{k'}^\circ \leq \mu_j^\circ$. Based on Lemma 1, we further have $\vartheta(\mu_j^\circ) \leq \vartheta(\mu_{k'}^\circ) = \vartheta(\mu_{k'}^\star) < f(\boldsymbol{\mu}^\star)$, and $f(\boldsymbol{\mu}^\circ) < f(\boldsymbol{\mu}^\star)$. Then we have $\max\{\vartheta(\mu_1^\circ), \ldots, \vartheta(\mu_K^\circ), f(\boldsymbol{\mu}^\circ)\} < f(\boldsymbol{\mu}^\star)$. Therefore, we obtain a smaller objective value of problem $(\mathcal{D}2)$, which contradicts the assumption that $\boldsymbol{\mu}^\star$ is optimal.

Second, consider $\vartheta(\mu_{k'}^\star) > f(\boldsymbol{\mu}^\star) \geq 0$. Then it follows that $\vartheta(\mu_{k'}^\star) = \max\{\vartheta(\mu_1^\star), \ldots, \vartheta(\mu_K^\star), f(\boldsymbol{\mu}^\star)\}$. Then we can obtain a new solution $\boldsymbol{\mu}^\dagger = [\mu_1^\dagger, \ldots, \mu_K^\dagger]^T$, i.e., $\mu_j^\dagger = \mu_j^\star, \forall j \in \mathcal{K} \setminus \mathcal{K}', \mu_{k'}^\dagger = \mu_{k'}^\star + \epsilon, \forall k' \in \mathcal{K}'$, where ϵ is sufficiently small such that $\mu_{k'}^\dagger < \mu_j^\dagger$ and $\vartheta(\mu_{k'}^\dagger) > f(\boldsymbol{\mu}^\dagger)$. Then we have $\max\{\vartheta(\mu_1^\dagger), \ldots, \vartheta(\mu_K^\dagger), f(\boldsymbol{\mu}^\dagger)\} = \vartheta(\mu_{k'}^\dagger) < \vartheta(\mu_{k'}^\star)$, where we have used Lemma 1. Therefore, we obtain a smaller objective value of problem $(\mathcal{D}2)$, i.e., $\vartheta(\mu_{k'}^\dagger)$, which contradicts the assumption that $\boldsymbol{\mu}^\star$ is optimal.

According to the above, we can replace μ_k by μ in $(\mathcal{D}2)$ and we have $(\mathcal{D}3): \min_{\mu\in\mathcal{X}} \max(\vartheta(\mu), \mu C)$. Obviously, the optimal μ is given by $\vartheta(\mu) = \mu C$, or i.e., $\kappa \ln(\frac{\kappa}{\mu}) - (\kappa - \mu) = \mu\tilde{C}$. Let $\chi \triangleq \frac{\kappa}{\mu}$. Then it can be expressed as $\chi \ln \chi - \chi + 1 = \tilde{C}$, whose optimal solution is given by [16] as $\chi^\star = \frac{\tilde{C}-1}{\mathcal{W}(\frac{\tilde{C}-1}{e})}$, where $\mathcal{W}(\cdot)$ is the Lambert W-Function [18]. From above, we can see that the optimal μ is given by $\mu^\star = \frac{\kappa\mathcal{W}(\frac{\tilde{C}-1}{e})}{\tilde{C}-1}$.

Appendix B
Proof of Proposition 2

By constraints (10a), the sum of τ_k is bounded by $p^\star \sum_{k=1}^K \tau_k \leq \sum_{k=1}^K \sum_{\omega=1}^\Omega \theta_{k\omega}\pi_\omega = \sum_{\omega=1}^\Omega \sum_{k=1}^K \theta_{k\omega}\pi_\omega \overset{(a)}{=} C\sum_{\omega=1}^\Omega \pi_\omega$, where (a) is due to the definition of C and $\theta_{k\omega}$, we have $\sum_{k=1}^K \theta_{k\omega} = C$, $\omega = 1, \ldots, \Omega$. Without loss of generality, we can set $\sum_{k=1}^K \tau_k = \frac{C\alpha}{p^\star}\sum_{\omega=1}^\Omega \pi_\omega$, where $\alpha \in (0, 1]$ is a constant scaler. Referring to constraint (10b), we have $\sum_{\omega=1}^\Omega \pi_\omega = \frac{1}{\frac{C\alpha}{p^\star}+1}$. Therefore, we have

$$\sum_{k=1}^K \tau_k = \frac{\frac{C\alpha}{p^\star}}{\frac{C\alpha}{p^\star}+1} \leq \frac{\frac{C}{p^\star}}{\frac{C}{p^\star}+1}. \tag{11}$$

The equality is achieved when $\alpha = 1$.

On the other hand, this optimal value can be achieved by arbitrarily choosing $\hat{\omega} \in \{1, \ldots, \Omega\}$, such that $\pi_{\hat{\omega}}^\star = \frac{p^\star}{C+p^\star}$, and $\pi_\omega^\star = 0, \forall \omega \in$

[2] One can easily see that $\mu_{k'} < \kappa$ for $\forall k' \in \mathcal{K}'$, otherwise we have $\vartheta(\mu_k) = 0$ for $\forall k \in \mathcal{K}$, which cannot be optimal.

[3] Note that $\vartheta(\mu_k)$ is a decreasing function for $\forall 0 < \mu_k < \kappa$.

$\{1, \ldots, \Omega\}, \omega \neq \hat{\omega}$. One can see that the constraints are not violated and the optimal value can be achieved.

Finally, substituting (11) into the objective function of problem (10) and using the fact that $e^{\mathcal{W}(x)} = \frac{x}{\mathcal{W}(x)}$, we can obtain Proposition 2.

REFERENCES

[1] Y. Xu, G. Gui, H. Gacanin, and F. Adachi, "A survey on resource allocation for 5G heterogeneous networks: Current research, future trends, and challenges," *IEEE Commun. Surv. Tut.*, vol. 23, no. 2, pp. 668–695, Apr.–Jun. 2021.

[2] Y. Xu and G. Gui, "Optimal resource allocation for wireless powered multicarrier backscatter communication networks," *IEEE Wireless Commun. Lett.*, vol. 9, no. 8, pp. 1191–1195, Aug. 2020.

[3] Q. Wu, L. Liu, and R. Zhang, "Fundamental trade-offs in communication and trajectory design for UAV-enabled wireless network," *IEEE Wireless Commun.*, vol. 26, no. 1, pp. 36-44, Feb. 2019.

[4] Q. Wu, Y. Zeng, and R. Zhang, "Joint trajectory and communication design for multi-UAV enabled wireless networks," *IEEE Trans. Wireless Commun.*, vol. 17, no. 3, pp. 2109–2121, Mar. 2018.

[5] Y. Zeng, Q. Wu, and R. Zhang, "Accessing from the sky: A tutorial on uav communications for 5G and beyond," *Proc. IEEE*, vol. 107, no. 12, pp. 2327–2375, Dec. 2019.

[6] L. Yu *et al.*, "Sparse code multiple access for 6G wireless communication networks: Recent advances and future directions," *IEEE Commun. Standards Mag*., vol. 5, no. 2, pp. 92–99, Jun. 2021.

[7] O. L. A. Lpez, H. Alves, R. D. Souza, S. Montejo-Snchez, E. M. G. Fernndez, and M. Latva-Aho, "Massive wireless energy transfer: Enabling sustainable IoT toward 6G era," *IEEE Internet Things J.*, vol. 8, no. 11, pp. 8816–8835, Jun. 2021.

[8] Z. Wang, W. Xu, D. Yang, and J. Lin, "Joint trajectory optimization and user scheduling for rotary-wing UAV-enabled wireless powered communication networks," *IEEE Access*, vol. 7, pp. 181369–181380, 2019.

[9] Z. Wang, M. Wen, S. Dang, L. Yu, and Y. Wang, "Trajectory design and resource allocation for UAV energy minimization in a rotary-wing UAV-enabled WPCN," *Alexandria Eng. J.*, vol. 60, no. 1, pp. 1787–1796, 2021.

[10] Z. Chen, K. Chi, K. Zheng, G. Dai, and Q. Shao, "Minimization of transmission completion time in UAV-enabled wireless powered communication networks," *IEEE Internet Things J.*, vol. 7, no. 2, pp. 1245–1259, Feb. 2020.

[11] Y. Xu, Z. Liu, C. Huang, and C. Yuen, "Robust resource allocation algorithm for energy harvesting-based D2D communication underlaying UAV-assisted networks," *IEEE Internet Things J.*, to be published, doi: 10.1109/JIOT.2021.3078264.

[12] L. Xie, J. Xu, and R. Zhang, "Throughput maximization for UAV-enabled wireless powered communication networks," *IEEE Internet Things J.*, vol. 6, no. 2, pp. 1690–1703, Apr. 2019.

[13] L. Xie, J. Xu, and Y. Zeng, "Common throughput maximization for UAV-enabled interference channel with wireless powered communications," *IEEE Trans. Commun.*, vol. 68, no. 5, pp. 3197–3212, May 2020.

[14] S. Cho, K. Lee, B. Kang, K. Koo, and I. Joe, "Weighted harvest-then-transmit: UAV-enabled wireless powered communication networks," *IEEE Access*, vol. 6, pp. 72212–72224, 2018.

[15] H. Ye, X. Kang, J. Joung, and Y. Liang, "Optimization for full-duplex rotary-wing UAV-enabled wireless-powered IoT networks," *IEEE Trans. Wireless Commun.*, vol. 19, no. 7, pp. 5057–5072, Jul. 2020.

[16] M. Jiang, Y. Li, Q. Zhang, and J. Qin, "Joint position and time allocation optimization of UAV enabled time allocation optimization networks," *IEEE Trans. Commun.*, vol. 67, no. 5, pp. 3806–3816, May 2019.

[17] W. Yu and R. Lui, "Dual methods for nonconvex spectrum optimization of multicarrier systems," *IEEE Trans. Commun.*, vol. 54, no. 7, pp. 1310–1322, Jul. 2006.

[18] R. M. Corless, G. H. Gonnet, D. E. G. Hare, D. J. Jeffrey, and D. E. Knuth, "On the lambertw function," *Adv. Comput. Math.*, vol. 5, no. 1, pp. 329–359, 1996.